

Artificial Electromagnetic Characteristics Analysis in Hyperbolic Metamaterials Slot Waveguides Based on Graphene

Xu Li, Lin Cheng*, Mingrui Yuan, Pengfei Cao, Xiaodong He, and Xiaoping Zhang

Abstract—In this paper, hyperbolic metamaterials slot waveguides based on graphene have been proposed to explore the optical characteristics. The hyperbolic metamaterials are composed of graphene-dielectric alternating multilayer. It has been verified in our proposed structure that the optical field is enhanced efficiently in the slot region, which results in the optical gradient force becoming larger as the distance of slot region becomes smaller. Both numerical simulation and theoretical analysis systematically reveal that the stronger gradient force can be achieved through smaller slot gap or lower chemical potential. Furthermore, the optical properties of two coupled waveguides have been studied under the relation of incident wavelength, chemical potential of graphene, composition of graphene-dielectric multilayer (e.g., number of periods, filling factor of graphene) of the waveguides in this work. We find that a larger gradient force can be obtained by adjusting the height of waveguides either decreasing the thickness of dielectric with constant number of periods or compressing the number of periods with fixed graphene filling factor. Our results will be helpful to the study of the optical field in the infrared region and also has great potentials in nanoscale manipulation and plasmonic devices.

1. INTRODUCTION

Artificial electromagnetic materials are man-made composite structures with powerful electromagnetic control ability. One type of anisotropic metamaterials, because of its special dispersion relation described as hyperbolic curves, is also called hyperbolic metamaterials [1]. Hyperbolic metamaterials offer potentials in negative refraction [2], subwavelength imaging [3] and photon density enhancement [4]. The hyperbolic metamaterials can be constructed by the metal-dielectric multilayer structure [5] or metal-dielectric nanowire structure [6]. However, considering practical applications, the permittivity of metal is hard to adjust and the optics loss of metal is also hard to overcome, which limits the application of hyperbolic metamaterials.

Graphene, a two-dimensional honeycomb lattice structure periodically lined by a single layer of carbon atoms, is authentic two-dimensional materials [7]. Compared with metal, the biggest advantage of graphene is that its surface conductivity can be adjusted by the gate voltage or chemical doping method [8–11], and its optics loss is rather low [12]. Recently, the graphene-germanium hyperbolic slot waveguides has been proposed, and the local field enhancement in the slot region at infrared frequencies had been investigated [13], which provides the basis for further study of gradient force in slot region. The enhancement of optical field in slot region can produce optical gradient force, which can be used as optical tweezers [14, 15]. Therefore, it is much worth discussing the optical force originated from graphene-dielectric multilayer structures with optical field enhancement in the slot region at infrared band.

In this paper, the properties of hyperbolic metamaterials slot waveguides constructed by graphene-dielectric multilayer have been discussed in two waveguide modes, and their high refractive index can

Received 30 September 2016, Accepted 3 November 2016, Scheduled 1 December 2016

* Corresponding author: Lin Cheng (chenglin@lzu.edu.cn).

The authors are with the School of Information Science and Engineering, Lanzhou University, Lanzhou 730000, China.

be used to explore the optical field in the slot region. In order to solve the problem that the metal is unsuited for the infrared band and unable to operate easily in potential operation, graphene is used in this work to substitute metal. Due to the rapid gradient change of the optical field in slot region of graphene-dielectric multilayer hyperbolic slot waveguides, the gradient force, which is calculated by using Maxwell's stress tensor integration, is much stronger than that in metal-dielectric multilayer slot waveguides. Furthermore, this proposed structure with no need for a special small slot gap g can achieve optical force in the same order of magnitudes as achieved by other slot waveguides. This is to say, under the condition of same slot gap g , the force of graphene-dielectric multilayer structure in this work is bigger than that in the metal-dielectric multilayer structure reported in [16]. Such graphene-based hyperbolic slot waveguides are useful in optical manipulation, such as driving the nanostructure [17] and optical transport of nanoparticles or biomolecules [18].

2. THEORETICAL MODEL AND ANALYSIS

The surface conductivity of graphene σ_g can be obtained from Kubo formalisms [19]:

$$\sigma_g = -j \frac{e^2}{4\pi\hbar} \ln \left[\frac{2|\mu_c| - (\omega - j/\tau)\hbar}{2|\mu_c| + (\omega - j/\tau)\hbar} \right] - j \frac{e^2 K_B T}{\pi\hbar^2 (\omega - j/\tau)} \left[\frac{\mu_c}{K_B T} + 2 \ln(e^{-\mu_c/K_B T} + 1) \right] \quad (1)$$

where K_B represents the reduced Planck's constant, μ_c the chemical potential, and e the charge of electron. Throughout this paper, we assume that the temperature $T = 300$ K, the relaxation time $\tau = 0.5$ ps, and ε_0 and ω are the permittivity of free space and angular frequency of incident light, respectively. The permittivity of graphene with the thickness of $t_g = 1$ nm can be equivalent to an isotropic permittivity tensor. The surface normal permittivity of graphene is $\varepsilon_{g,n} = 1$, and the in-plane permittivity of graphene can be defined as [20]:

$$\varepsilon_{g,t} = \varepsilon_{g,n} - j\sigma_g/\omega\varepsilon_0 t_g \quad (2)$$

As shown in Fig. 1(a), the hyperbolic metamaterial waveguide system is composed of two graphene-dielectric alternative multilayers with height H and width W vertically aligned with a gap distance g . Here, SiO_2 ($\varepsilon_d = 2.2$) is chosen to be the dielectric layer and constructed with graphene to form hyperbolic metamaterials. Because the incident wavelength at infrared frequencies is much larger than the period of multilayer structure ($t = 10$ nm), the hyperbolic metamaterials can be treated as a homogeneous effective medium, and the permittivity tensor of different directions can be defined as [21]:

$$\varepsilon_x = \varepsilon_z = f_g \varepsilon_{g,t} + (1 - f_g) \varepsilon_d, \quad \varepsilon_y = \frac{\varepsilon_{g,n} \varepsilon_d}{f_g \varepsilon_d + (1 - f_g) \varepsilon_{g,n}} \quad (3)$$

where filling factor of graphene is $f_g = t_g/t$. According to the effective medium theory (EMT), the parallel permittivities ε_x and ε_z of the hyperbolic metamaterials should be negative while the vertical permittivity ε_y should be positive, i.e., $\text{Re}(\varepsilon_x) < 0$ and $\text{Re}(\varepsilon_y) > 0$. The effective permittivity of multilayer structure along x , y and z directions as functions of wavelength and chemical potential μ_c are demonstrated in Fig. 1(b) and Fig. 1(d). Here, $f_g = t_g/t = 0.1$, $\varepsilon_y = 1.9643$ and $\text{Re}(\varepsilon_x) < 0$ which form the hyperbolic metamaterials. Meanwhile, the conductivity of graphene depends on incident wavelength, and chemical potentials μ_c are shown in Fig. 1(c) and Fig. 1(e). The hyperbolic dispersion of the graphene-dielectric multilayer metamaterials can be described as [22]:

$$\frac{k_x^2 + k_z^2}{\varepsilon_y} - \frac{k_y^2}{|\varepsilon_x|} = k_0^2 \quad (4)$$

where k_x , k_y and k_z denote the wave vectors of different directions, and k_0 is the free-space wave vector related to the incident wavelength.

When two waveguides get close to each other, it will cause strong mode coupling and result in two eigenmodes including symmetric mode (denoted by Ms) and anti-symmetric mode (denoted by Ma). In the condition of incident wavelength $\lambda_0 = 20$ μm , the chemical potential $\mu_c = 0.8$ eV and the slot gap $g = 10$ nm, and the electric field component E_y and the magnetic field component H_x corresponding to the two eigenmodes are obtained by numeric simulation with software COMSOL MULTIPHYSICS as shown in Fig. 2.

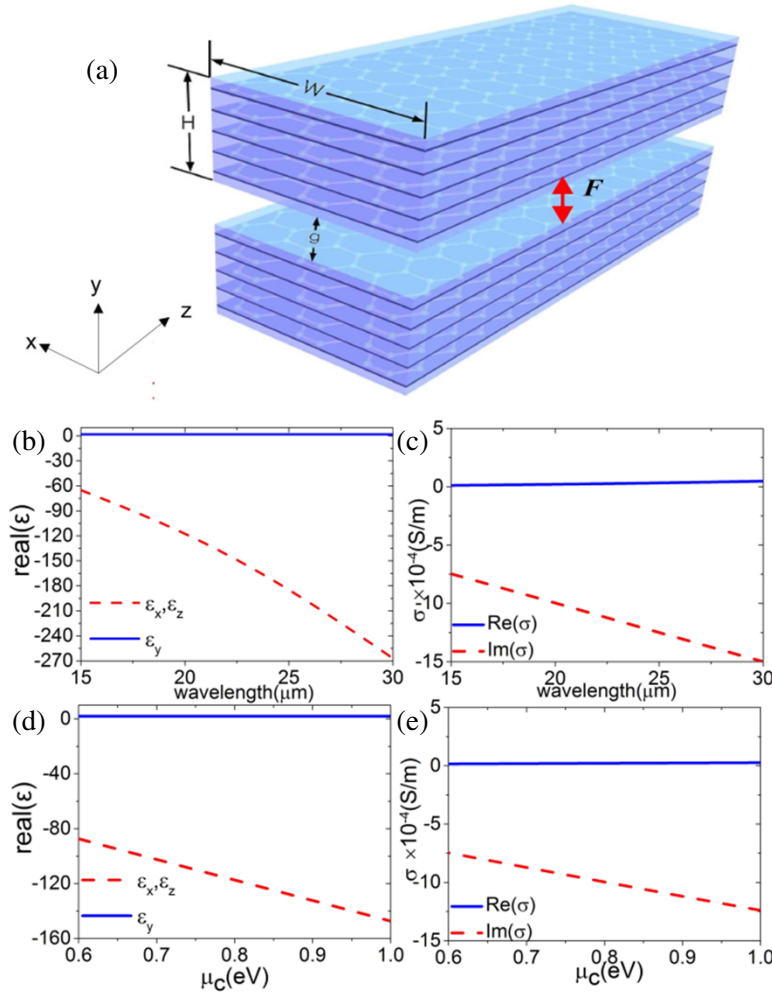


Figure 1. (a) The schematic view of hyperbolic metamaterials slot waveguides based on graphene. The effective permittivity of multilayer structure along x , y and z direction varied with incident wavelength (b) and chemical potential μ_c (d). The conductivity of graphene depends on incident wavelength and chemical potentials μ_c are shown in (c) and (e), respectively.

Given the height of each waveguide $H = 100$ nm and the width $W = 120$ nm. Obviously, the optics field intensity is increased significantly in slot region for the symmetric mode M_s , because of the constructively interfered electric field. On the contrary, for the anti-symmetric mode M_a , the optical field intensity is weak due to the destructively interfered electric field. The optical field intensity at the slot region directly indicates the magnitude of transverse optical forces between the two coupled waveguides; therefore, the optical force for the mode M_s is expected to be much stronger than that for the mode M_a .

In order to explore the principle of electric field enhancement, the changes of real modal index and optical propagation lengths have been demonstrated numerically under different conditions. As we know, the effective refractive index along the propagation direction can be achieved through $n_{eff,z} = k_z/k_0$ while the optical propagation lengths $L = \lambda/4\pi\text{Im}(n_{eff,z})$. Fixing the filling ratio of graphene $f_g = 0.1$, two types of height $H = 100$ nm and $H = 50$ nm are compared in the following. Because the surface conductivity of graphene can be adjusted by the gate voltage, when the chemical potential μ_c increases, the real modal index decreases quickly (see Fig. 3(a)) and optical propagation length L becomes larger (see Fig. 3(b)). As shown in Figs. 3(c) and (d), real modal index and optical propagation lengths change smoothly along with the incident wavelength. When the slot gap g is enlarged, the real modal index

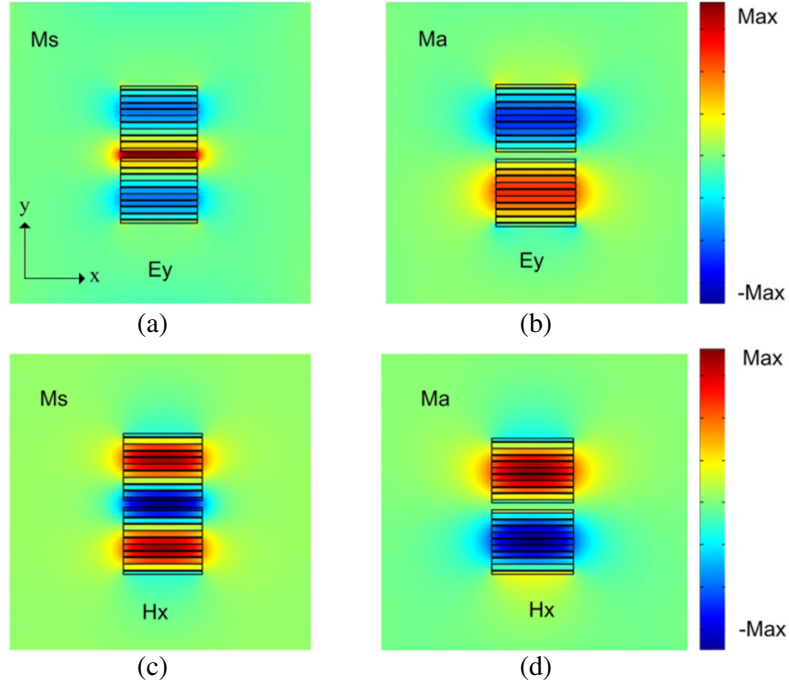


Figure 2. The electric field component E_y of mode Ms (a) and mode Ma (b). The magnetic field component H_x of mode Ms (c) and mode Ma (d). Here, $H = 100$ nm, $W = 120$ nm, $g = 10$ nm and $\mu_c = 0.8$ eV.

increases gently in mode Ma but decreases severely in mode Ms as shown in Fig. 3(e). Meanwhile, the propagation length increases rapidly in mode Ms but decreases stably in mode Ma as shown in Fig. 3(f). As shown in Fig. 3(e) and Fig. 3(f), the two coupling modes (Ms and Ma) become convergence with increase of the slot gap g , so $g = 110$ nm is the approximate limit of the coupling phenomena between our hyperbolic metamaterials slot waveguides based on graphene. The real modal index and optical propagation lengths are susceptible to slot gap and chemical potential, which are easy to control in the practical operation. Moreover, we can also find that the real modal index of mode Ms is always bigger than that of mode Ma . So the symmetric mode will be beneficial for further boosting the optical force in slot waveguide structures.

Also the slot waveguides system can be analyzed by using the theoretical analysis in 2D coupled slab waveguides approximation model. Based on the continuity of field components E_z and H_x on the interface, the propagation constant β can be obtained [23]:

$$\tan\left(-k_y \frac{H}{2} + \varphi\right) = -\frac{\gamma \varepsilon_z}{k_y} \tanh\left(\gamma \frac{g}{2}\right), \quad \tan\left(k_y \frac{H}{2} + \varphi\right) = \frac{\gamma \varepsilon_z}{k_y} \quad (5)$$

$$\frac{\beta^2}{\varepsilon_y} + \frac{k_y^2}{\varepsilon_z} = k_0^2, \quad \beta^2 - \gamma^2 = k_0^2 \quad (6)$$

where γ is the decay rate in air and φ the phase shift in the center of one waveguide. Owing to the small coupling in the gap region of mode Ma and because the gradient force is so weak that we ignore the condition of mode Ma , only the gradient force of mode Ms is analyzed in this paper. After solving

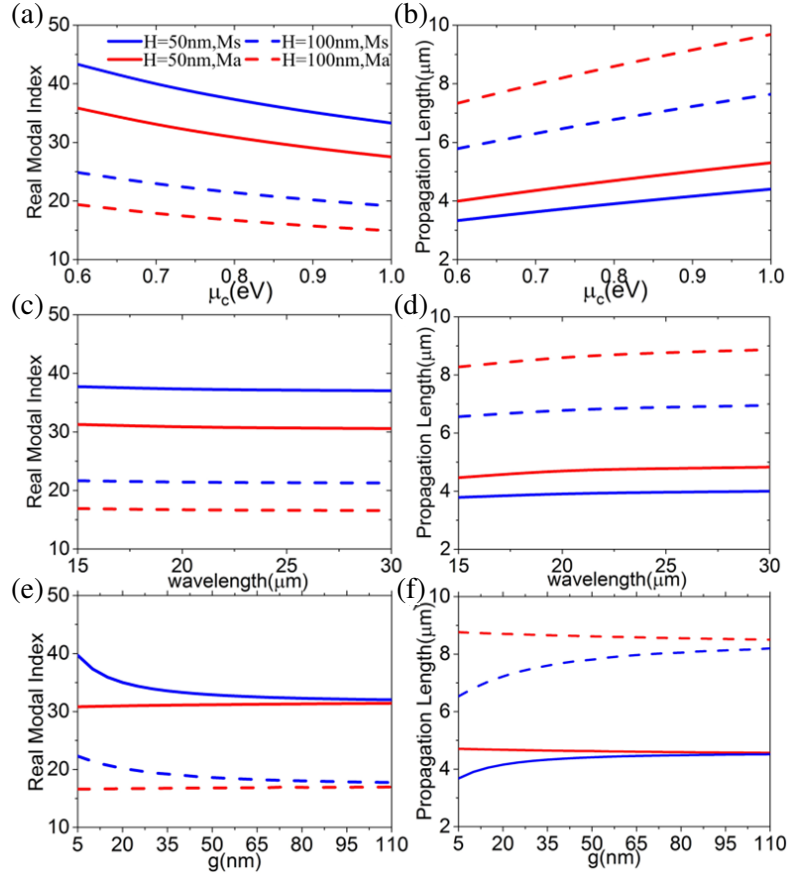


Figure 3. The dependencies of real modal index (a), (c), (e) and propagation length (b), (d), (f) under different conditions. In (a) and (b), the chemical potential μ_c varies while the incident wavelength is $\lambda_0 = 20 \mu\text{m}$ and the slot gap $g = 10 \text{ nm}$. In (c) and (d), the wavelength varies while the chemical potential $\mu_c = 0.8 \text{ eV}$ and the slot gap $g = 10 \text{ nm}$. In (e) and (f), the slot gap varies while the incident wavelength is $\lambda_0 = 20 \mu\text{m}$ and the chemical potential $\mu_c = 0.8 \text{ eV}$.

the above equations, the results of mode Ms should be taken into field expressions:

$$E_y = B_0 \begin{cases} \cos\left(-k_y \frac{H}{2} + \varphi\right) \frac{\cosh(\gamma y)}{\cosh\left(\gamma \frac{g}{2}\right)}, & 0 < |y| < \frac{g}{2} \\ \frac{1}{\varepsilon_y} \cos\left[k_y \left(|y| - \frac{H+g}{2}\right) + \varphi\right], & \frac{g}{2} < |y| < \frac{g}{2} + H \\ \cos\left(k_y \frac{H}{2} + \varphi\right) \exp\left[-\gamma \left(|y| - \frac{g}{2} - H\right)\right], & |y| > \frac{g}{2} + H \end{cases} \quad (7)$$

$$E_z = B_0 \begin{cases} -j \frac{\gamma}{\beta} \cos\left(-k_y \frac{H}{2} + \varphi\right) \frac{\sinh(\gamma y)}{\cosh\left(\gamma \frac{g}{2}\right)}, & 0 < |y| < \frac{g}{2} \\ j \frac{k_y}{\beta \varepsilon_y} \sin\left[k_y \left(|y| - \frac{H+g}{2}\right) + \varphi\right], & \frac{g}{2} < |y| < \frac{g}{2} + H \\ j \frac{\gamma}{\beta} \cos\left(k_y \frac{H}{2} + \varphi\right) \exp\left[-\gamma \left(|y| - \frac{g}{2} - H\right)\right], & |y| > \frac{g}{2} + H \end{cases} \quad (8)$$

$$H_x = B_0 \begin{cases} \frac{w\varepsilon_0}{\beta} \cos\left(-k_y \frac{H}{2} + \varphi\right) \frac{\cosh(\gamma y)}{\cosh\left(\gamma \frac{g}{2}\right)}, & 0 < |y| < \frac{g}{2} \\ \frac{w\varepsilon_0}{\beta\varepsilon_y} \cos\left[k_y \left(|y| - \frac{H+g}{2}\right) + \varphi\right], & \frac{g}{2} < |y| < \frac{g}{2} + H \\ \frac{w\varepsilon_0}{\beta} \cos\left(k_y \frac{H}{2} + \varphi\right) \exp\left[-\gamma \left(|y| - \frac{g}{2} - H\right)\right], & |y| > \frac{g}{2} + H \end{cases} \quad (9)$$

where $B_0^2 = P/(\int \text{Re}((H_x) * (E_y)/2) ds)$, and the normalized energy flow is $P = 1$ in the integration area [24].

Due to the great change of the vertical permittivity ε_y between air and waveguides, the optical field is enhanced in the slot region of mode M_s . The optical gradient force can be calculated by the integration of Maxwell's stress tensor $T_{ij} = \varepsilon_0(E_i E_j - \delta_{ij} E^2/2) + \mu_0(H_i H_j - \delta_{ij} H^2/2)$ [25]. By taking field expressions into the Maxwell's stress tensor, the optical gradient force along y direction can be expressed as:

$$F_y = \frac{\oint_S T_{ij} dS}{P_z} e_y \quad (10)$$

where S is the closed surface that encircles single waveguide.

As shown in Fig. 4, the results calculated by numeric simulation method and theoretical analysis method are compared. Fig. 4(a) and Fig. 4(c) show that the real modal index depends on slot gap g and chemical potential μ_c , respectively. Fig. 4(b) shows that the optical gradient force becomes larger as the gap distance g becomes smaller, because the coupling strength of two waveguides is getting much stronger as the distance of two waveguides is getting much smaller. Therefore, this big optical force can be obtained in the slot region by the coupling of two waveguides in the infrared field. Note that when $g = 110$ nm, the gradient force is close to zero, which reconfirms that the slot gap limit is 110 nm approximately in our structure. The optical gradient force also decreases with the increase of chemical

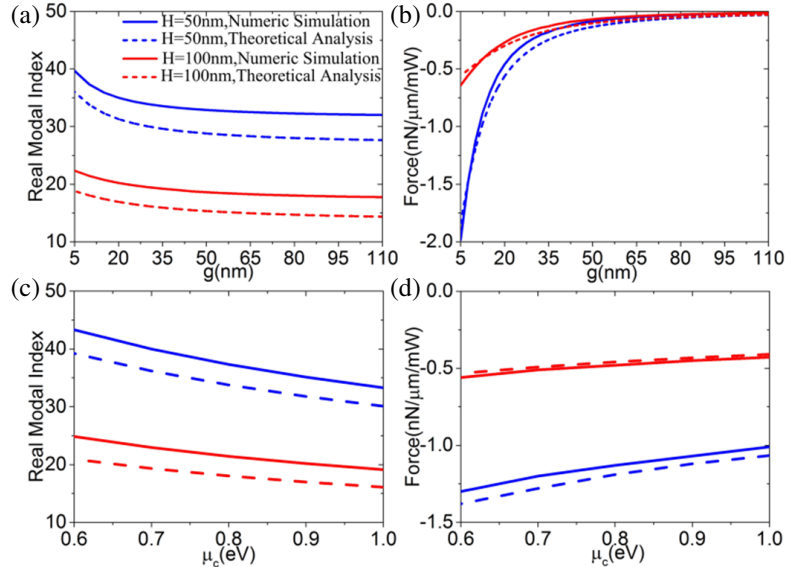


Figure 4. The calculated real modal index and optical gradient force in hyperbolic slot waveguides with different slot gap g in (a) and (b), and with varied chemical potential μ_c in (c) and (d), respectively. Both numeric simulation (solid lines) and theoretical analysis (dotted lines) are shown in figures with the fixed incident wavelength $\lambda_0 = 20 \mu\text{m}$. The chemical potential is $\mu_c = 0.8 \text{ eV}$ in (a) and (b). The slot gap is $g = 10 \text{ nm}$ in (c) and (d).

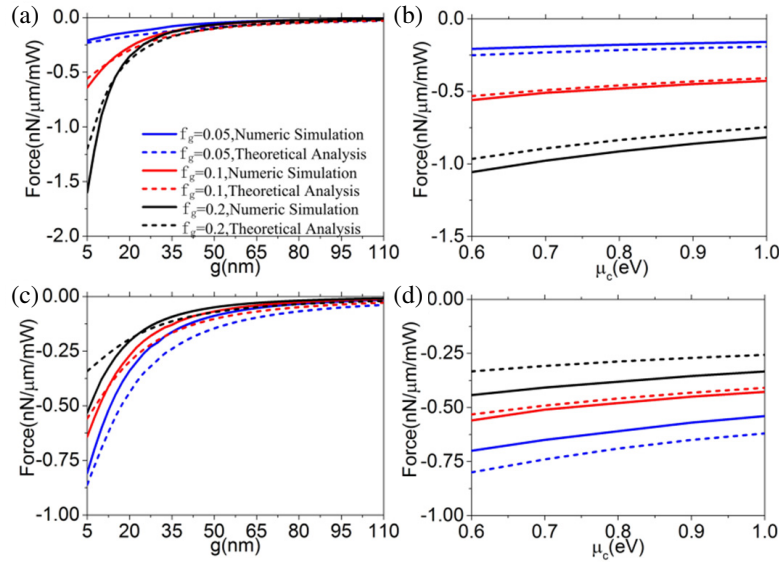


Figure 5. The optical gradient force in hyperbolic slot waveguides with different filling factor of graphene is calculated under slot gap g in (a) and (c) and varied chemical potential μ_c in (b) and (d), respectively. Both numeric simulation (solid lines) and theoretical analysis (dotted lines) are shown in figures with the fixed incident wavelength $\lambda_0 = 20 \mu\text{m}$. The chemical potential is $\mu_c = 0.8 \text{ eV}$ in (a) and (c) and the slot gap is $g = 10 \text{ nm}$ in (b) and (d). (a) and (b) show the calculated gradient force in the same number of periods $n = 10$. (c) and (d) show the calculated gradient force in the same height of waveguides $H = 100 \text{ nm}$.

potential μ_c as shown in Fig. 4(d). Therefore, the gradient force can be changed by adjusting slot gap g and chemical potential μ_c .

Here, due to the absolute condition of theoretical analysis calculation, the real modal index in numeric simulation is a little bit bigger than that in theoretical analysis with the same waveguide height H . This is because the theoretical analysis is calculated with infinite width in 2D coupled slab waveguides approximation model and the numeric simulation calculated with finite width. Therefore, due to the influence of width of waveguides, the real modal index in numeric simulation and theoretical analysis cannot be fully consistent. Meanwhile, the calculation process of optical force can eliminate the effects from different methods, so the results calculated by two methods basically tally with each other. As shown in Fig. 4, the optical gradient force of $H = 50 \text{ nm}$ is always bigger than that of $H = 100 \text{ nm}$. It is mainly because the real modal index is always bigger, and the coupling strength is stronger when the waveguide height is smaller. Beyond that, the gradient force becomes bigger with the decrease of the slot gap. The field enhancement is confined completely in the slot region, for slot gap $g = 5 \text{ nm}$, and the distance between adjacent graphene layers is 9 nm , which is bigger than the distance adopted in previous discussions [26–29] between two coupled structures, so the quantum effect can be neglected in this work.

In practical operation, the thickness of graphene is not easy to change, so different coupling phenomena can be studied by adjusting the thickness of dielectric, which is equal to changing filling factor of graphene f_g . So keeping the thickness of graphene $t_g = 1 \text{ nm}$ constant, three kinds of filling factor $f_g = 0.05, 0.1$ and 0.2 , denoting the corresponding thickness of dielectric $19 \text{ nm}, 9 \text{ nm}$ and 4 nm are compared in Fig. 5. As shown in Fig. 5(a), the gradient force is calculated by both numeric method and theoretical method with the same number of periods ($n=10$). Due to the same number of periods when the filling factors are $f_g = 0.05, f_g = 0.1$ and $f_g = 0.2$, the heights of waveguides are $H = 200 \text{ nm}, H = 100 \text{ nm}$ and $H = 50 \text{ nm}$, respectively. Obviously, the gradient force is much stronger with a larger filling factor ($f_g = 0.2$) or a smaller height of waveguide ($H = 50 \text{ nm}$) when the number of periods is the same. On the contrary, given the height of waveguides ($H = 100 \text{ nm}$) and adjusting the number of periods, the gradient force is also calculated in three kinds of f_g by both numeric method and theoretical

method as shown in Fig. 5(c). Because of the same height of waveguides, when the numbers of periods $n = 5$, $n = 10$ and $n = 20$, respectively, the filling factors of graphene are corresponding to $f_g = 0.05$, $f_g = 0.1$ and $f_g = 0.2$. The gradient force is much stronger in $f_g = 0.05$ than that in $f_g = 0.2$ when height of waveguides is fixed. The optical gradient force always decreases with the increase of the chemical potential μ_c as shown in Fig. 5(b) and Fig. 5(d). Therefore, the number of periods n and the height of waveguides H (or the filling factor of graphene f_g) have effect on the optical gradient force, which are the key parameters in studying and applying hyperbolic metamaterials slot waveguides.

3. CONCLUSIONS

In conclusion, we study the real modal index and propagation length of the hyperbolic metamaterials slot waveguides based on graphene between symmetric mode and anti-symmetric mode. Compared to hyperbolic metamaterials slot waveguides with metal-dielectric multilayer, graphene-dielectric multilayer are quite easy to construct and have a lower intrinsic loss. Moreover, it is more flexible to regulate the optical properties of hyperbolic metamaterials slot waveguides based on graphene by external conditions, such as incident wavelength, chemical potential, number of periods, thickness of dielectric (or filling factor of graphene) and height of waveguides, to achieve a bigger gradient force in infrared band. By taking the field expressions into the Maxwell's stress tensor, we not only calculate the gradient force by theoretical method, but also verify the results with numerical simulation. Further, we find that keeping the number period unchanged, the gradient force becomes stronger as the height of waveguides decreases, or keeping the height of waveguides unchanged, the gradient force becomes stronger as the graphene filling factor shrinks. Our research supplies the reference value in actual operation in future work. Therefore, such characteristics of hyperbolic metamaterials slot waveguides based on graphene can be useful in optical transport of nanoparticles or bio-sensor in infrared field.

ACKNOWLEDGMENT

This work is supported in part by the Fundamental Research Funds for the Central Universities under Grant No. lzujbky-2016-143, lzujbky-2016-138, and lzujbky-2015-306.

REFERENCES

1. Barnakov, Y. A., H. Li, E. E. Narimanov, M. A. Noginov, T. Tumkur, and G. Zhu, "Bulk photonic metamaterial with hyperbolic dispersion," *Applied Physics Letters*, Vol. 94, No. 15, 151105–151105-3, 2008.
2. Yao, J., Z. Liu, Y. Liu, Y. Wang, C. Sun, G. Bartal, A. M. Stacy, and X. Zhang, "Optical negative refraction in bulk metamaterials of nanowires," *Science*, Vol. 321, No. 5891, 930, 2008.
3. Wood, B., J. B. Pendry, and D. P. Tsai, "Directed sub-wavelength imaging using a layered metal-dielectric system," *Physics*, 2006, doi:10.1103/PhysRevB.74.1151163.
4. Jacob, Z., J. Y. Kim, G. V. Naik, A. Boltasseva, E. E. Narimanov, and V. M. Shalaev, "Engineering photonic density of states using metamaterials," *Applied Physics B*, Vol. 100, No. 1, 215–218, 2010.
5. Mei, Z. L., Y. L. Xu, J. Bai, and T. J. Cui, "Nonmagnetic electromagnetic transparent wall realized by a metal-dielectric multilayer structure," *Optics Express*, Vol. 20, No. 15, 16955–16967, 2012.
6. Starkobowes, R., J. Atkinson, W. Newman, H. Hu, T. Kallos, G. Palikaras, R. Fedosejevs, S. Pramanik, and Z. Jacob, "Optical characterization of epsilon-near-zero, epsilon-near-pole, and hyperbolic response in nanowire metamaterials," *Journal of the Optical Society of America B*, Vol. 32, No. 10, 2015.
7. Cui, J. P., W. S. Zhao, W. Y. Yin, J. Hu, "Signal transmission analysis of multilayer graphene nanoribbon (MLG NR) interconnects," *IEEE Transactions on Electromagnetic Compatibility*, Vol. 54, No. 1, 126–132, 2012.
8. Fei, Z., A. S. Rodin, G. O. Andreev, and W. Bao, "Gate-tuning of graphene plasmons revealed by infrared nano-imaging," *Nature*, Vol. 487, No. 7405, 82–85, 2012.

9. Liu, H., Y. Liu, and D. Zhu, "Chemical doping of graphene," *Journal of Materials Chemistry*, Vol. 21, No. 10, 3335–3345, 2011.
10. Guo, B., L. Fang, B. Zhang, J. R. Gong, "Graphene doping: A review," *Sciences Journal*, Vol. 1, No. 2, 80–89, 2011.
11. Ballestar, A., P. Esquinazi, J. Barzola-Quiquia, S. Dusari, F. Bern, R. R. D. Silva, et al., "Possible superconductivity in multi-layer-graphene by application of a gate voltage," *Carbon*, Vol. 72, No. 2, 312–320, 2014.
12. Ju, L., B. Geng, L. Horng, C. Girit, M. Martin, Z. Hao, H. A. Bechtel, X. Liang, A. Zettl, Y. R. Shen, "Graphene plasmonics for tunable terahertz metamaterials," *Nature Nanotechnology*, Vol. 6, No. 10, 630–634, 2011.
13. Zhu, B., G. Ren, Y. Gao, Y. Yang, B. Wu, Y. Lian, and S. Jian, "Local field enhancement in infrared graphene-dielectric hyperbolic slot waveguides," *IEEE Photonic Technology Letters*, Vol. 27, No. 3, 276–279, 2015.
14. Yang, X., Y. Liu, R. F. Oulton, X. Yin, and X. Zhang, "Optical forces in hybrid plasmonic waveguides," *Nano Letter.*, Vol. 11, No. 2, 321–328, 2011.
15. Ginis, V., P. Tassin, C. M. Soukoulis, and I. Veretennicoff, "Enhancing optical gradient forces with metamaterials," *Physical Review Letter*, Vol. 110, No. 5, 66–71, 2013.
16. He, Y., S. He, J. Gao, and X. Yang, "Giant transverse optical forces in nanoscale slot waveguides of hyperbolic metamaterials," *Optics Express*, Vol. 20, No. 20, 22372–22382, 2012.
17. Zhao, Q., C. Guclu, Y. Huang, F. Capolino, and O. Boyraz, "Silicon nitride waveguides for plasmon optical trapping and sensing applications," *Physics*, 2015.
18. Yang, A. H. J., S. D. Moore, B. S. Schmidt, M. Klug, M. Lipson, and D. Erickson, "Optical manipulation of nanoparticle biomolecules in sub-wavelength slot waveguides," *Nature*, Vol. 457, No. 7225, 71–75, 2009.
19. Zhang, T., L. Chen, and X. Li, "Graphene-based tunable broadband hyperlens for far-field subdiffraction imaging at mid-infrared frequencies," *Optics Express*, Vol. 21, No. 18, 20888–20899, 2013.
20. Wang, B., X. Zhang, X. Yuan, and J. Teng, "Optical coupling of surface plasmons between graphene sheets," *Applied physics Letter*, Vol. 100, No. 13, 131111–131114, 2012.
21. Sun, Y., Z. Zheng, J. Cheng, G. Sun, and G. Qiao, "Highly efficient second harmonic generation in hyperbolic metamaterials slot waveguides with large phase matching tolerance," *Optics Express*, Vol. 23, No. 5, 6370–6378, 2015.
22. Shekhar, P., J. Atkinson, and Z. Jacob, "Hyperbolic metamaterials: fundamentals and applications," *Physics*, Vol. 1, No. 1, 1–17, 2014.
23. He, Y., S. He, and X. Yang, "Optical field enhancement in nanoscale slot waveguides of hyperbolic metamaterials," *Optics Letters*, Vol. 37, No. 14, 2907–2909, 2012.
24. Almeida, V. R., Q. Xu, C. A. Barrios, and M. Lipson, "Guiding and confining light in void nanostructure," *Optics Letters*, Vol. 29, No. 11, 1209–1211, 2004.
25. Novotny, L., B. Hecht, and O. Keller, *Principles of Nano-optics*, Cambridge University Press, Vol. 60, No. 7, 41, 2012.
26. Esteban, R., A. G. Borisov, P. Nordlander, and J. Aizpurua, "Bridging quantum and classical plasmonics with a quantum-corrected model," *Nature Communications*, Vol. 3, No. 3, 199–202, 2012.
27. Marinica, D. C., A. K. Kazansky, P. Nordlander, J. Aizpurua, and A. G. Borisov, "Quantum plasmonics: nonlinear effects in the field enhancement of a plasmonic nanoparticle dimer," *Nano Letters*, Vol. 12, No. 3, 1333–9, 2012.
28. Teperik, T. V., P. Nordlander, J. Aizpurua, and A. G. Borisov, "Quantum effects and nonlocality in strongly coupled plasmonic nanowire dimers," *Optics Express*, Vol. 21, No. 22, 27306–25, 2013.
29. Thongrattanasiri, S., A. Manjavacas, and F. J. G. D. Abajo, "Quantum finite-size effects in graphene plasmons," *Acs Nano*, Vol. 6, No. 2, 1766–75, 2012.